Title	Bridge roughness index as an indicator of bridge dynamic amplification
Authors(s)	O'Brien, Eugene J., Li, Yingyan, González, Arturo
Publication date	2006-05
Publication information	O'Brien, Eugene J., Yingyan Li, and Arturo González. "Bridge Roughness Index as an Indicator of Bridge Dynamic Amplification" 84, no. 12 (May, 2006).
Publisher	Elsevier
Item record/more information	http://hdl.handle.net/10197/2532
Publisher's statement	All rights reserved.
Publisher's version (DOI)	10.1016/j.compstruc.2006.02.008

Bridge Roughness Index as an Indicator of Bridge Dynamic Amplification

Eugene OBrien, Yingyan Li and Arturo González
Department of Civil Engineering, University College Dublin, Earlsfort Terrace, Dublin 2, Ireland

ABSTRACT

The concept of a road roughness index for bridge dynamics is developed. The International Roughness Index (IRI) is shown to be very poorly correlated with bridge dynamic amplification as it takes no account of the location of individual road surface irregularities. It is shown in this paper that a Bridge Roughness Index (BRI) is possible for a given bridge span which is a function only of the road surface profile and truck fleet statistical characteristics. The index is a simple linear combination of the changes in road surface profile; the coefficients are specific to the load effect and span of interest. The BRI is well correlated with bridge dynamic amplification for bending moment due to 2-axle truck crossing events. A similar process can be used to develop a BRI for trucks with other numbers of axles or combinations of trucks meeting on a bridge.

Keywords: DAF, DAE, BRI, dynamic, roughness, bridge, vehicle.

Corresponding author: Li Yingyan
E-mail: yingyan.li@ucd.ie
Tel: +353-1-716-7281
Fax: +353-1-716-7399

1. Introduction

The Dynamic Amplification Factor (DAF) for a bridge is defined as the maximum total (dynamic plus static) load effect divided by the maximum static load effect. DAF is influenced by many factors. Speed is particularly important, as noted by many authors [1-6] and in particular the ratio of speed to bridge 1st natural frequency [7]. Road roughness is also a key factor [3-4, 8], particularly for short bridges.

In the highway industry, indices for the evaluation of pavement surface evenness have been developed since the 1960s. The most popular parameters are the International Roughness Index (IRI) [9-11] which was developed and recommended by the World Bank to evaluate pavement roughness, and the Power Spectral Density (PSD) [12].
[Li – can you fix up the ref numbering please]
Olsson (1985), Lin (1997), Henchi et al. (1997), Liu et al. (2002) and Majumder and Manohar (2003) are just some of the authors that use finite element analysis with six degrees of freedom per node to model bridges dynamically. Olsson (1985) compared the results of finite element analysis with an Euler-Bernoulli beam model [Li – did he compare them?]. Green and Cebon (1994) modelled two bridges in the U.K. with finite elements and compared the results to field measurements. [Li – I think this is true – is it?] Chompooming and Yener (1995) present a finite element model of a beam and slab bridge. This type of section is also modeled by Kou and Dewolf (1997) who use plate elements for the deck and beam elements for the girders. González (2001) couples displacements and velocities at the bridge/vehicle contact points at each time step in an iterative formulation. Yau and Yang (2004) allow for instability and inertial effects in a finite element model of a cable stayed bridge.

The effect of road surface irregularities on bridge vibration has been examined by DIVINE [1], Green et al. [4], Lay and Zhu [13], Kou and Dewolf [14], Lei and Noda [15] and Chatterjee et al. [16]. Vehicle and bridge models have been used to simulate the vehicle-bridge interaction system and to determine the effect of profile unevenness. However, these papers investigate the influence of different PSD levels. It has been found by Li et al. [17] that there are substantial differences in dynamic amplification between road profiles with the same PSD level and the same IRI value.

Michaltsos [18] and Pesterev et al. [19, 20] have shown that the position of an irregularity is important for bridge dynamic amplification. In a previous paper [17], the authors confirm this and show that if bridge deflections are negligible [20], the principle of superposition applies for the dynamic response to individual road surface irregularities. This makes possible the estimation of dynamic amplification by adding together the DAFs due to each irregularity that makes up the road surface profile. Very good agreement with critical DAF values is reported for a range of 'good' road surface profiles. A significant problem is that the resulting dynamic amplification estimate is specific to the properties (spring stiffness etc.) of that vehicle.

Yang et al. [12], Zhu & Law [21] and Brady & OBrien [22] examine cases of two following loads and compare the effects to single load crossings. Axle spacing is identified as being particularly important [22, 23] and it quickly becomes clear that an amplification factor derived from a 1-axle vehicle model is of limited value as an indicator of DAF for multiple-axle vehicles.

The goal of this paper is to develop the concept of a Bridge Roughness Index (BRI) which can be used as an estimator of DAF for a given vehicle class, and in particular in this paper, a BRI for 2-axle vehicles. The BRI will be a function of the road profile only; it will not be dependent on the speeds or properties of particular vehicles. A BRI potentially constitutes an extremely useful measure of road surface roughness that could be used by bridge maintenance managers as an indicator of the level of dynamic amplification that might be expected on a bridge.

2. BRIDGE VIBRATION

2.1. Vehicle-bridge interaction model

A half-car model crossing a simply supported Bernoulli-Euler beam at a constant speed is used to simulate 2-axle vehicle events (Fig. 1). The motion controlling this system is defined by the ordinary differential equations [24]:

$$-I\frac{d^2\varphi(t)}{dt^2}+(-1)^i D_i(Z_i(t)+Z_{bi}(t))=0 \tag{1a}$$

$$-m_3\frac{d^2 y_3(t)}{dt^2}-\sum_{i=1}^{2}[Z_i(t)+Z_{bi}(t)]=0 \tag{1b}$$

$$m_{3i}g+m_i g-m_i\frac{d^2 y_i(t)}{dt^2}+Z_i(t)+Z_{bi}(t)-R_i(t)=0 \qquad i=1,2 \tag{1c}$$

$$EJ\frac{\partial^4 v(x,t)}{\partial x^4}+\mu\frac{\partial^2 v(x,t)}{\partial t^2}+2\mu\omega_b\frac{\partial\ v(x,t)}{\partial t}=\sum_{i=1}^{2}\varepsilon_i\delta(x-x_i)R_i(t) \tag{1d}$$

where I and $\varphi(t)$ are the mass moment of inertia and rotational degree of freedom of the body mass respectively; D_i is the horizontal distance between the centroid of sprung mass and unsprung mass i; m_1, m_2, m_3 are masses of the front axle, rear axle and vehicle

body respectively and $y_1(t)$, $y_2(t)$ and $y_3(t)$ are the corresponding vertical displacement of their centers of gravity; g is acceleration of gravity; $v(x,t)$ is the displacement of the bridge at location x and time t; E, J, μ and ω_b are modulus of elasticity, inertia of the cross-section, mass per unit length and circular frequency of damping of the bridge respectively; ε_i.= 1 if axle i is present on the bridge and ε_i.= 0 if not; $\delta(x\text{-}x_i)$ is the Dirac function. Therefore,

$$Z_i(t) = K_s\left[y_{3i}(t) - y_i(t)\right] \tag{2a}$$

is the force in the spring between the ith axle and the vehicle body, where K_s is the suspension spring stiffness.

$$Z_{bi}(t) = C_s\left[\frac{dy_{3i}(t)}{dt} - \frac{dy_i(t)}{dt}\right] \tag{2b}$$

is the damping force between the ith axle and the vehicle body, where C_s is a suspension linear damper.

$$y_{3i}(t) = y_3(t) - (-1)^i D_i \varphi(t) \tag{2c}$$

is the displacement of the contact point between the ith axle and the vehicle body.

$$\begin{aligned} m_{31} &= m_3 \frac{D_2}{D_1 + D_2} \\ m_{32} &= m_3 \frac{D_1}{D_1 + D_2} \end{aligned} \tag{2d}$$

are the masses of the sprung part of the vehicle by axle.

$$R_i(t) = K_t\left[y_i(t) - \varepsilon_i v(x_i, t) - r(x_i)\right] \geq 0 \tag{2e}$$

is the tire force imparted to the bridge by the ith axle, where K_t is tire stiffness and $r(x_i)$ is height of road profile at location of axle i. No allowance has been made for separation

of the tire from the road. Based on the work of Frýba [24], numerical results are found in the time domain through the Runge-Kutta-Nyström method [25].

2.2. Dynamic Amplification due to 2-axle vehicle

In a previous study [17], the authors have proven that the effect of individual road irregularities can be superposed for a quarter-car model traveling on a short-span bridge with a good road profile. Bending moment is found by adding the moment due to the vehicle traveling on a perfectly smooth surface and the moment due to each individual irregularity that exists on the surface. The approach is accurate for negligible bridge deflections and a good approximation when bridge deflections are small compared to the road irregularities. Based on this assumption of superposition, the total normalized midspan bending moment, $M(c,t)$, for a vehicle speed, c, and position of 1st axle x_1, can be calculated as

$$M(c,x_1) = M_0(c,x_1) + \sum_{i=1}^{N}\left[M_u(c,i,x_1) - M_0(c,x_1)\right] \times s(i) \tag{3}$$

where M_0 is the normalized midspan bending moment caused by the vehicle on a smooth profile and M_u is the normalized midspan moment due to a unit ramp at location i. The profile is discretized into N ramps each 100 mm long and the measured fall in the ith ramp in mm is $s(i)$. All bending moments are normalized by dividing them by the maximum static bending moment. The calculation procedure is illustrated in Fig.2 for a road profile made of two ramps of heights H_1 and $-H_2$ located at -0.1 and 0 m respectively. The total moment M due to a vehicle of given mechanical parameters and speed (Fig.2(a)) is the result of adding three moments: (1) M_0 corresponding to a smooth profile (Fig.2(b)), (2) $[s(1)\times(M_{u(x=-0.1)}-M_0)]$, or moment due to a unit ramp at x =

-0.1 (Fig.2(c)) scaled by the height of the first ramp ($s(1) = H_1/0.001$), and (3) [$s(2)\times(M_{u(x=0)}-M_0)$], or moment due to a unit ramp at $x = 0$ (Fig.2(d)) scaled by its height ($s(2) = -H_2/0.001$). This approach involves the addition of bending moment values corresponding to different critical points near the centre of the bridge. Then, the dynamic amplification factor due to a vehicle traveling at speed c can be estimated from the maximum normalized total moment for any location x_1 while the vehicle is near the center of the bridge:

$$DAE(c) = \max_{0.4L \le x_1 \le 0.8L} \left[M(c, x_1) \right] \tag{4}$$

It becomes clear that the nature of a given road profile relating bridge dynamics, can only be characterized as 'good' or 'poor' linked to a given vehicle type.

Unfortunately, while *DAE* provides an excellent estimate of dynamic amplification for a particular vehicle, it is only accurate for that vehicle. For example, on the road profiles described as Fig. 3, the 2-axle estimator is illustrated for three vehicles with axle spacings D (=5 m), $0.7D$ and $1.3D$ in Fig. 4. Clearly the spacing used to generate the terms, $M_0(c)$ and $M_u(c,i)$ in Eq. (3), has a most significant influence on the result. Further, there is no one spacing for a 2-axle vehicle that will provide good estimates of dynamic amplification for other vehicle spacings.

DAF and *DAE* are also strongly influenced by vehicle speed. The normalized bending moment due to the two-axle vehicle defined by parameters in Table 1 and traveling on a smooth road profile, $M_0(c, x_1)$, is illustrated in Fig. 5(a) for $x_1 = 0.5L$, i.e., front axle at

the center of the bridge. The corresponding normalized moments for unit ramp excitations of the vehicle, $M_u(c,i,0.5L) - M_0(c,0.5L)$, are given in Fig. 5(b). This graph provides a valuable insight into the source of the total bending moment. It can be seen that particular locations on the bridge are especially important. For example a ramp at -0.4*L* is highly significant while a ramp at -0.2*L* makes no contribution. It can also be seen that there are positive and negative effects – light and dark zones in the figure. Hence the effects of some ramps will cancel out while others will be additive and there will be particular combinations of ramps that will result in very high bending moment.

A section through Fig. 5(b) corresponding to a speed of 80 km/h is illustrated in Fig. 6(a). The product of this graph and the road profile of Fig. 3 is illustrated in Fig. 6(b). The sum of all ordinates in the latter graph represents the total contribution of the road profile to the normalized bending moment (see Eq. (3)). It can be seen that bending and hence dynamic amplification is highly sensitive to the location of road surface irregularities. The corresponding graph for a speed of 120 km/h, illustrated in Fig. 6(c), shows the sensitivity to speed.

3. MONTE CARLO SIMULATION

It has been shown that dynamic amplification and the estimate of dynamic amplification provided by *DAE* for a given vehicle, is strongly influenced by the inter-axle spacing and speed of that vehicle. Similar variability in results can be shown for other vehicle properties such as the ratio of the axle weights. A *BRI* does not need to be accurate but

must provide an indication of DAF for the range of vehicles and speeds that are likely to occur on the bridge.

To overcome the problem of multiple parameters, statistical data is used to determine the properties of 'typical' vehicles from a truck fleet. For this paper, truck fleet statistics were obtained from a Weigh-in-Motion station on the A1 road near Ressons in France. Data was collected over a period of 105 hours for 9498 trucks. Only 2-axle trucks of more than 15 tonne gross vehicle weight were considered. The histograms for gross vehicle weight, spacing, axle weight ratio and speed are illustrated in Fig. 7.

Monte Carlo simulation [26] is used to generate 2-axle truck properties representative of the measured data. This is achieved by a simple bootstrapping from the measured data, i.e., frequency is selected by generating a random number between zero and $\sum_i f_i$, where f_i is the frequency of interval i; the property from the corresponding interval in the histogram is then used in the simulation. While there may be some correlation between vehicle properties, all properties are assumed to be independent in this study. For each of 21 values of x_1 in the interval $0.4L \leq x_1 \leq 0.8L$, 500 sets of property values were generated and the mean and standard deviation for $M_0(x_1)$ calculated. The results are illustrated in Fig. 8(a) and Fig. 8(c). Fig. 8(a) corresponds to some extent to a truck fleet equivalent of Fig. 5(a) – it represents the mean normalized moment on a smooth road profile for 500 trucks with speeds, axle spacings etc. that are typical of the fleet. However, while Fig. 5(a) provides the maximum normalized moment for a range of speeds and front axle at midspan, Fig. 8(a) provides the vehicle at all points, averaged over many speeds and other vehicle parameters. Hence it gives an indication of the

mean dynamic amplification that might be expected of 2-axle vehicles, if the road profile were smooth. For example, when the front axle is located at the center of the bridge ($x_1 = 0.5L$), the mean normalized midspan moment, $\bar{M}(0.5L)$, is 0.8501, which means that the mean midspan moment from the 500 trucks/speeds considered is 0.8501 of the static value.

Fig. 8(b) is in some sense the truck fleet equivalent of Fig. 5(b). It gives the mean moment due to a unit ramp only at a given point from a representative sample of 500 trucks/speeds for a range x_1 of vehicle locations. Figs. 8(c) and (d) give the corresponding standard deviations of normalized bending moment: $M_0^{SD}(x_1)$ and $[M_u(x_1) - M_0(x_1)]^{SD}$ respectively.

Fig. 8 is used to evaluate the Bridge Roughness Index, *BRI*, for a given vehicle class, defined as:

$$BRI = \max_{0.4L \le x_1 \le 0.8L} \left[\bar{M}(x_1) + M^{SD}(x_1) \right] \tag{5}$$

where,

$$M_r(i, x_1) = M_u(i, x_1) - M_0(x_1) \tag{6a}$$

$$\bar{M}(x_1) = \bar{M}_0(x_1) + \sum_{i=1}^{N} \left[\bar{M}_r(i, x_1) \times s(i) \right] \tag{6b}$$

$$M^{SD}(x_1) = \sqrt{\left[M_0^{SD}(x_1) \right]^2 + \sum_{i=1}^{N} \left\{ \left[M_r^{SD}(i, x_1) \right]^2 \times \left[s(i) \right]^2 \right\}} \tag{6c}$$

The *BRI* represents a kind of mean estimate of dynamic amplification for vehicle properties and speeds representative of site measurements of key vehicle properties. Of course, considerable inaccuracy is introduced by taking the maximum of many averaged

components instead of averaging the maxima. However, this is necessary as it is only in this way that the *BRI* can be evaluated directly from a knowledge of Fig. 8 and the road profile, $s(i)$.

4. APPLICATION AND ASSESSMENT OF BRI

The application of the *BRI* is illustrated using the road profile of Fig. 3. The contribution of the different vehicles on a smooth profile can be seen to be varying from about 0.85 to 0.99 in the range of 0.5*L* to 0.75*L* as described in Fig. 8(a). The influence of the road profile roughness is illustrated in Fig. 9(a), which gives a positive contribution of up to 0.02 at the critical position of 0.68*L*, and the negative contribution at the position of 0.6*L*. Fig. 9(b) provides a breakdown of the contributions of the ramps that make up the profile to the mean normalized moment, namely, $\bar{M}_r(i, x_1) \times s(i)$. It is interesting to note that for this particular road profile, irregularities in the approach and at the start of the bridge are not significant (this would of course be different if there were large irregularities due to damage at a joint). The most important contributions of the road profile to bending moment occur in the range of 0.3*L* to 0.6*L* and depend on the location of the critical moment. At the time when $x_1 = 0.68L$, the critical point for this example, the contributions are illustrated in Fig. 9(c). Taking into account the standard deviation of the normalized bending moment, the dynamic amplification in Equ. 5 is described as Fig. 9(d), where the maximum value of 1.04 at the critical position of 0.7*L* represents *BRI*.

The accuracy of the *BRI* as a measure of profile roughness is assessed through comparison with DAF for 500,000 vehicle/speed/profile combinations. For this purpose, one thousand random road profiles are simulated with the Class 'B' [27, 28]. Together, the profiles represent a wide range of conditions with different positions of the ramps. For each road profile, 500 sets of vehicle properties are generated by Monte Carlo simulation. In all cases, the exact dynamic amplification, DAF, is calculated for comparison. The DAF is related to IRI in Fig. 10(a). Each point in this figure corresponds to one road profile, the mean of DAF plus the standard deviation is plotted against the IRI. It can be seen that there is no discernable correlation between IRI and DAF. (However, it is of note that better correlation is evident if a wider range of road roughnesses is considered). The coefficient of correlation for this set of Class 'B' profiles is 0.185. The ratio of DAF to *BRI* is illustrated in Fig. 10(b). While there is considerable scatter, there is a clear correlation and the correlation coefficient is 0.762.

The effect of road roughness is strongly influenced by the span of bridge considered. Figs. 11(a) and (b) give the mean normalized moment on a smooth profile and due to a unit ramp for a 15 m bridge respectively (equivalent of Figs. 8(a) and (b)). While Fig. 11(a) is similar to Fig. 8(a), considerable differences are evident in Figs. 8(b) and 11(b) in the magnitudes of the effects of unit ramps. The corresponding standard deviation of normalized moment caused by the 2-axle truck fleet when ignoring and taking into count the road roughness are shown in Figs. 11(c) and (d) respectively. Nevertheless, the principle of superposition still applies and the *BRI* has a good correlation with DAF as can be seen in Fig. 12.

5. DISCUSSION AND CONCLUSIONS

The concept of a bridge roughness indes, *BRI*, is developed in this paper. It is shown that IRI is poorly correlated with dynamic amplification for roads of average roughness. While there is considerable scatter in the relationship between the proposed *BRI* and dynamic amplification, this index is well correlated and considerably more so than IRI.

The index is independent of individual vehicle properties such as speed and axle spacing but is a function of the vehicle fleet properties, represented by histograms (Fig. 8). For a given bridge, it is calculated from the profile information only using factors derived from the fleet histograms, represented here by Fig. 7. Once the fleet-specific factors are known, the calculation of the *BRI* is quite simple (Eq. (5)).

The *BRI* factors developed here are applicable to 2-axle vehicles over 15 tonnes and to mid-span bending moment in 25 m simply supported bridges. It is shown that the corresponding factors for a 15 m bridge are quite different. Clearly the same procedure can be used to develop similar factors for other fleets, spans and load effects. For example, it would be straightforward to develop factors for 5-axle trucks representative of Western European highway traffic. This could be repeated for a number of spans and load effects. However, this would still only represent an indicator of dynamic amplification for a single truck crossing event and would not be accurate for two or more trucks meeting or passing on the bridge. The great variety of combinations of truck speeds, properties and other parameters is such that there appears to be no simple roughness measure of a road surface that is universally applicable and has a strong correlation with dynamic amplification. Nevertheless, the *BRI* is valuable in that it gives insight into the contribution that road roughness makes to dynamics. The importance of

irregularity location and the sensitivity of dynamic amplification to irregularities at particular points both on and in the approach to the bridge are identified.

REFERENCES

[1] DIVINE Programme, OECD, Dynamic Interaction of Heavy Vehicles with Roads and Bridges. DIVINE Concluding Conference. Ottawa, Canada, 1997.

[2] Olsson M. On the Fundamental Moving Load Problem. J Sound Vib 1991; 154(2):299-307.

[3] Liu C, Huang D, Wang TL. Analytical dynamic impact study Based on Correlated Road Roughness. Computers & Structures 2002; 80:1639-1650.

[4] Green MF, Cebon D, Cole DJ. Effects of Vehicle Suspension Design on Dynamics of Highway Bridges. J Struct Eng, ASCE, 1995; 121(2):272-282.

[5] Greco A, Santini. Dynamic Response of a Flexural non-classically Damped Continuous Beam Under Moving Loadings. Computers & Structures 2002; 80:1945-1953.

[6] Fafard M, Bennur M, Savard M. A General Multi-Axle Vehicle Model to Study the Bridge-Vehicle Interaction. Eng Comput 1997; 15(5):491-508.

[7] Brady SP, OBrien EJ, Žnidarič A. The Effect of Vehicle Velocity on the Dynamic Amplification of a Vehicle crossing a Simply Supported Bridge. J Bridge Eng, ASCE, 2005; accepted for publication.

[8] Coussy O, Said M, Van Hoove JP. The influence of Random Surface Irregularities on the Dynamic Response of Bridges under Suspended Moving Loads, J Sound Vib 1989; 130(2):313-320.

[9] Gillespie TD, Sayers MW, Segel L. Calibration of response-type pavement roughness measuring systems. National Cooperative Highway Research Program. Res.

Rep. No. 228, Transportation Research Board. National Research Council. Washington DC, 1980.

[10] Gillespie TD, Karimihas SM, Cebon D, Sayers M, Nasim MA, Hansen W, Ehsan N. Effects of heavy-vehicle characteristics on pavement response and performance. National Cooperative Highway Research Program. Res. Rep. No. 353, Transportation Research Board, National Research Council. Washington DC, 1993.

[11] Marcondes JA, Snyder MB, Singh SP. Predicting vertical acceleration in vehicles through pavement roughness. J Transport Eng, ASCE, 1992; 118(1):33-49.

[12] Yang YB and Lin BH. Vehicle-Bridge Analysis by Dynamic Condensation Method. J Struct Eng, ASCE, 1995; 121(11):1636-1643.

[13] Law SS, Zhu XQ. Bridge dynamic responses due to road surface roughness and braking of vehicle. J Sound Vib 2005; 282(3-5):805-830.

[14] Kou JW, Dewolf JT. Vibration Behavior of continuous span highway bridge-influencing variables. J Struct Eng, ASCE, 1997;123(3):333-344.

[15] Lei X, Noda NA. Analyses of Dynamic Response of Vehicle and Track Coupling System with Random Irregularity of Track Vertical Profile. J Sound Vib 2002; 258(1):147-165.

[16] Chatterjee PK, Datta TK, Surana CS. Vibration of Continuous Bridges Under Moving Vehicles. J Sound Vib 1994; 169(5):619-632.

[17] Li YY, OBrien EJ, González A. The Development of a Dynamic Amplification Estimator for Bridges with Good Road Profiles. J Sound Vib, in press, 2005.

[18] Michaltsos GT. Parameters Affecting the Dynamic Response of Light (Steel) Bridges. Facta Universitatis, Series Mechanics, Automatic Control and Robotics 2000; 2(10):1203-1218.

[19] Pesterev AV, Bergman LA, Tan CA. A novel approach to the calculation of pothole-induced contact forces in MDOF vehicle models. J Sound Vib 2004; 275(1-2):127-149.

[20] Pesterev AV, Bergman LA, Tan CA, Yang B. Assessing tire forces due to roadway unevenness by the pothole dynamic amplification factor method. J Sound Vib 2005; 279(3-5): 817-841.

[21] Zhu XQ, Law SS. Dynamic Load on Continuous Multi-Lane Bridge Deck From Moving Vehicles. J Sound Vib 2002; 251(4):697-716.

[22] Brady SP, OBrien EJ. The Effect of Vehicle Velocity on the Dynamic Amplification of Two Vehicles crossing a Simply Supported Bridge. J Bridge Eng, ASCE, 2005; accepted for publication.

[23] Yang YB, Yau JD, Wu YS. Vehicle-Bridge Interaction Dynamics With Applications to High-Speed Railways. Singapore: World Scientific Publishing Co. Pte. Ltd, 2004.

[24] Frýba L. Vibration of Solids and Structures under Moving Loads. Noordhoff International Publishing. Groningen. The Netherlands. 1972.

[25] Kreyszig E. ADVANCED ENGINEERING MATHEMATICS. New York: John Wiley & Sons Inc, 1983.

[26] Metcalfe AV. Statistics in Civil Engineering. New York: John Wiley & Sons Inc, 1997.

[27] ISO 8608. Mechanical vibration-Road surface profiles-reporting of measure data, 1995.

[28] González A, Development of Accurate Methods of Weighing Trucks in Motion, PhD. Thesis, Department of Civil Engineering, Trinity College, Dublin, Ireland, 2001.

Fig. 1 Schematic of the two-axle vehicle and bridge interaction system
Fig. 2 Concept of superposition of unit ramps: (a) Total moment. (b) Moment due to a smooth profile. (c) Moment due to a unit ramp at the first location. (d) Moment due to a unit ramp at the second location.
Fig. 3 Road Profile adjacent to and on the bridge (0 corresponds to the start of the bridge)
Fig. 4 Influence of axle spacing on dynamic amplification
Fig. 5 (a) Normalised moment for smooth surface and a range of speeds (front axle at mid-span). (b) Normalised moment for a range of unit ramp locations and speeds (front axle at mid-span)
Fig. 6 (a) Contribution to dynamic amplification due to a range of unit ramp locations for vehicle travelling at 80 km/h. (b) Contribution to dynamic amplification due to each road irregularity in 3(a) for vehicle at 80 km/h. (c) Contribution to dynamic amplification due to each road irregularity in 3(a) for vehicle at 90 km/h.
Fig. 7 Histograms of gross vehicle weights, axle spacings, axle weight distribution and speeds for a two-axle truck fleet.
Fig. 8 Normalized mid-span moments in a 25 m bridge due to a truck fleet: (a) Mean normalized moment for smooth surface and a range of vehicle locations. (b) Mean normalized moment for a range of vehicle and unit ramp locations. (c) Standard deviation of normalized moment for smooth surface and a range of vehicle locations. (d) Standard deviation of normalised moment for a range of vehicle and unit ramp locations.
Fig. 9 (a) Mean contribution to dynamic amplification due to road profile in Fig. 3 for a range of vehicle locations. (b) Mean contribution to dynamic amplification due to each road irregularity for a range of vehicle locations. (c) Mean contribution to dynamic amplification due to each road irregularity when front axle is at 0.68*L*. (d) Total mean plus the standard deviation normalised moment due to the road profile.
Fig. 10 (a) DAF versus IRI for a 25 m bridge. (b) DAF versus *BRI* for a 25 m bridge
Fig. 11 Normalized mid-span moments in a 15 m bridge due to a truck fleet: (a) Mean normalized moment for smooth surface and a range of vehicle locations. (b) Mean normalized moment for a range of vehicle and unit ramp locations. (c) Standard deviation of normalized moment for smooth surface and a range of vehicle locations. (d) Standard deviation of normalised moment for a range of vehicle and unit ramp locations.
Fig. 12 (a) DAF versus IRI for a 15 m bridge. (b) DAF versus *BRI* for a 15 m bridge

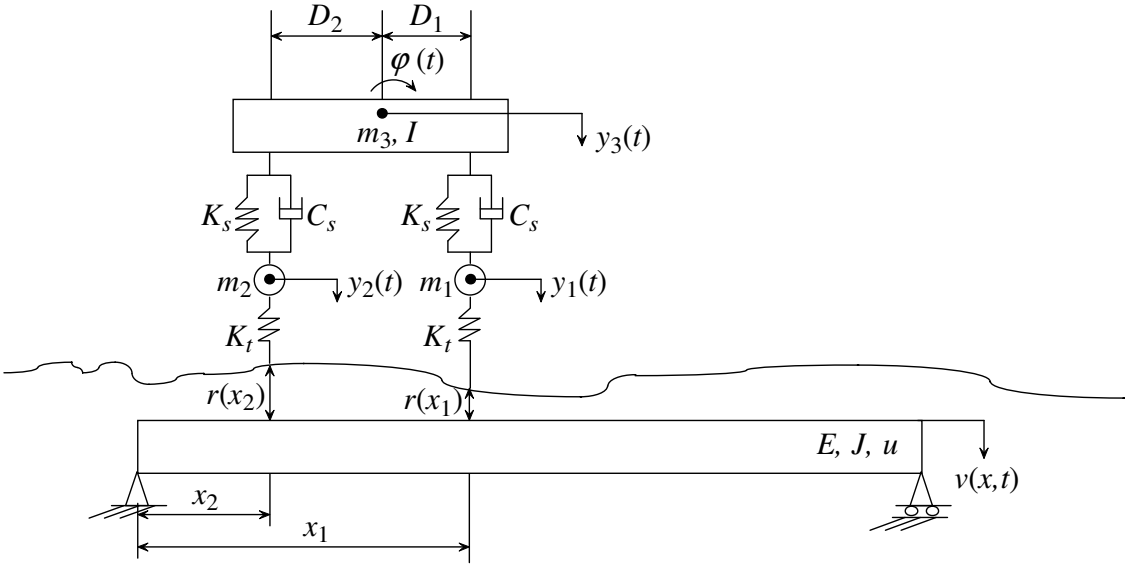
D_2
D_1
$\varphi(t)$
m_3, I
$y_3(t)$
K_s
C_s
K_s
C_s
m_2
$y_2(t)$
m_1
$y_1(t)$
K_t
K_t
$r(x_2)$
$r(x_1)$
E, J, u
$v(x,t)$
x_2
x_1

Fig. 1

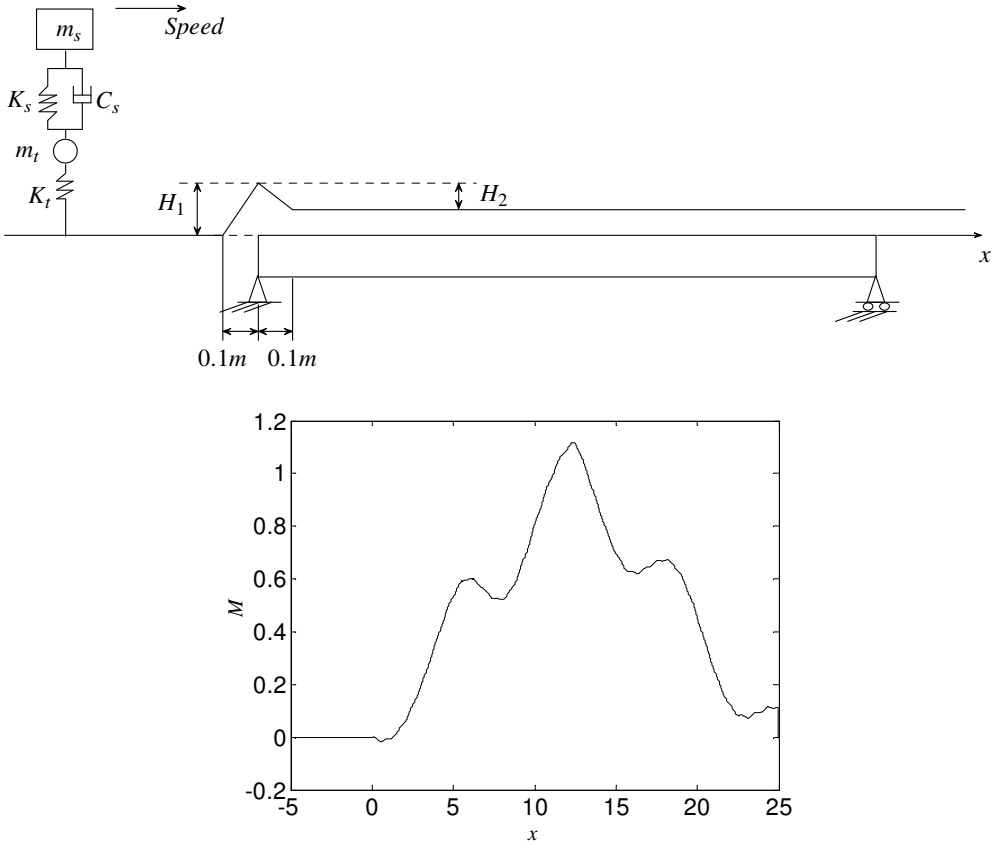

(a)

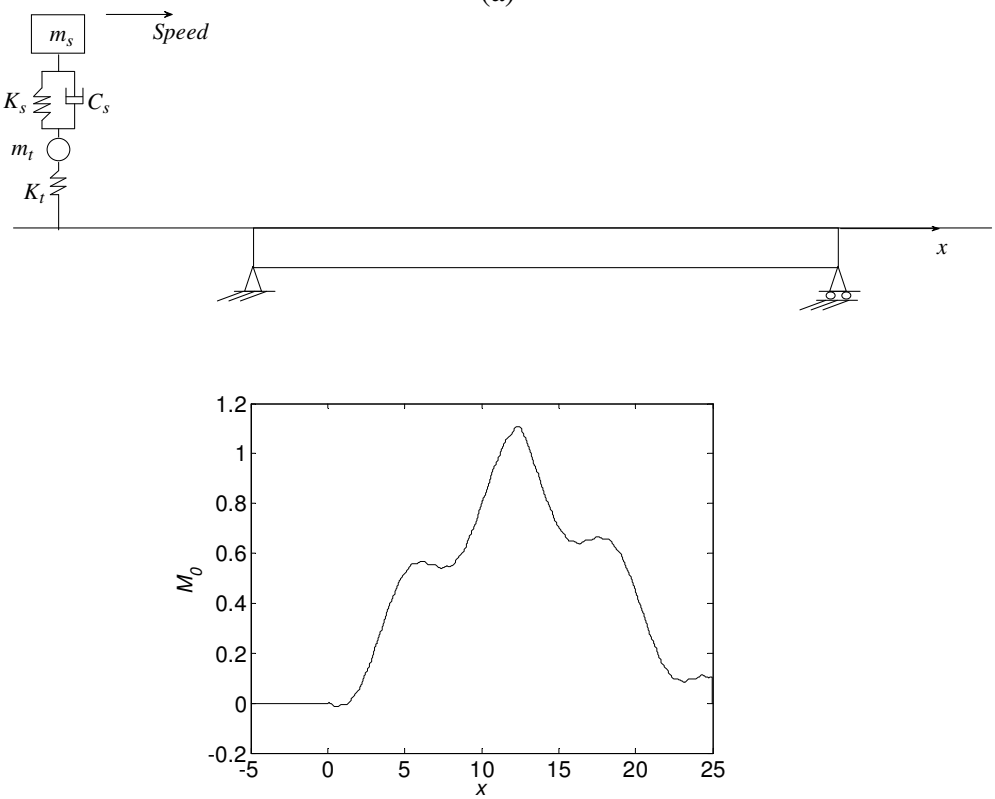

(b)

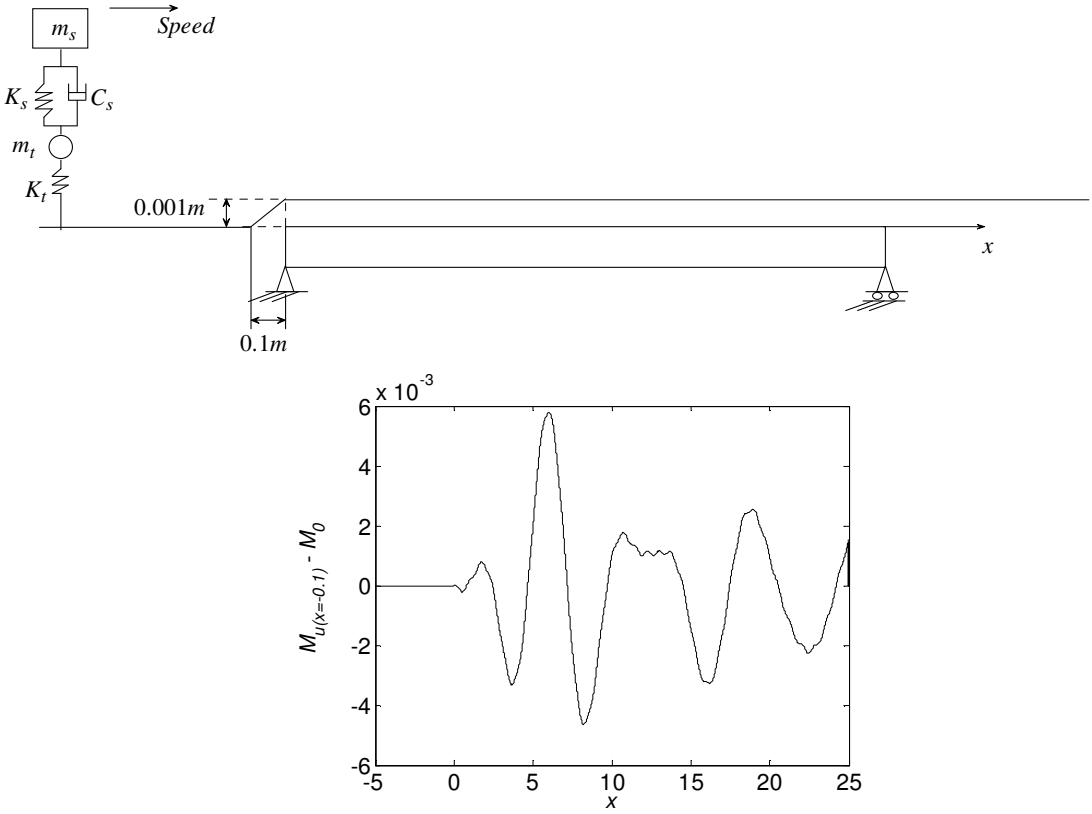
m_s
Speed
K_s
C_s
m_t
K_t
0.001m
x
0.1m
x 10^{-3}
$M_{u(x=-0.1)} - M_0$
x

(c)

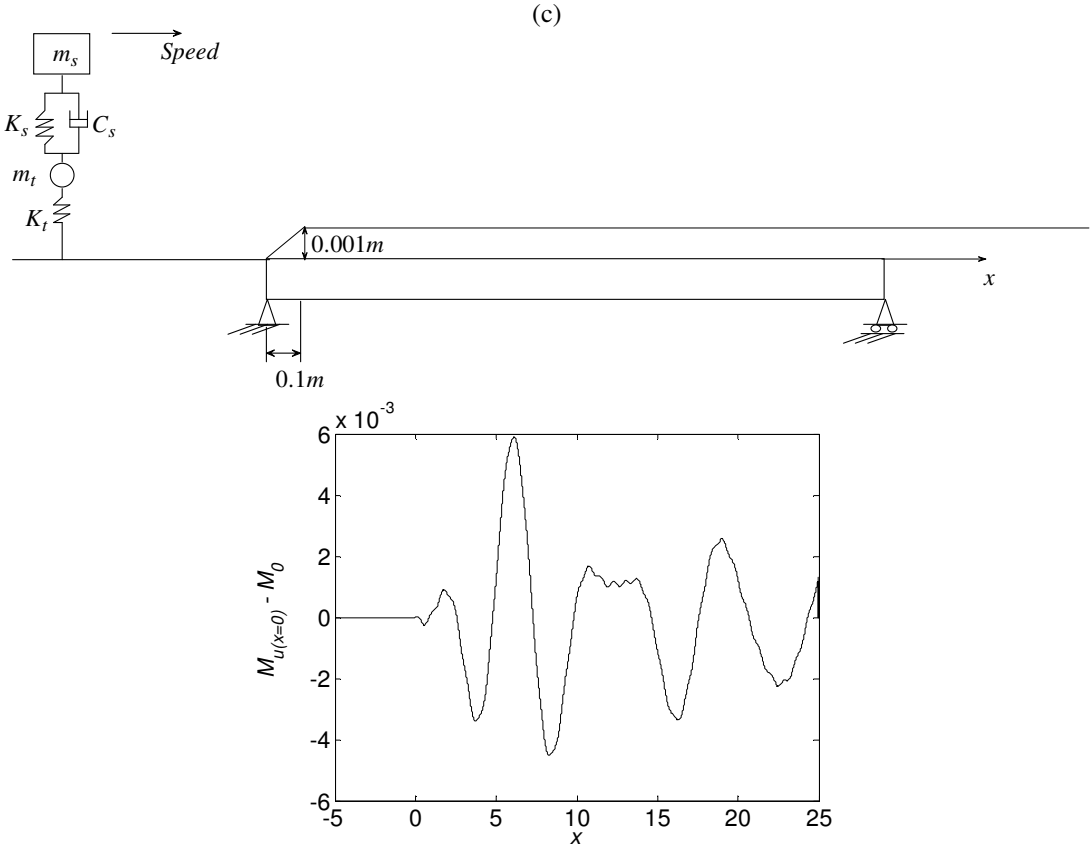
m_s
Speed
K_s
C_s
m_t
K_t
0.001m
x
0.1m
x 10^{-3}
$M_{u(x=0)} - M_0$
x

(d)

Fig. 2

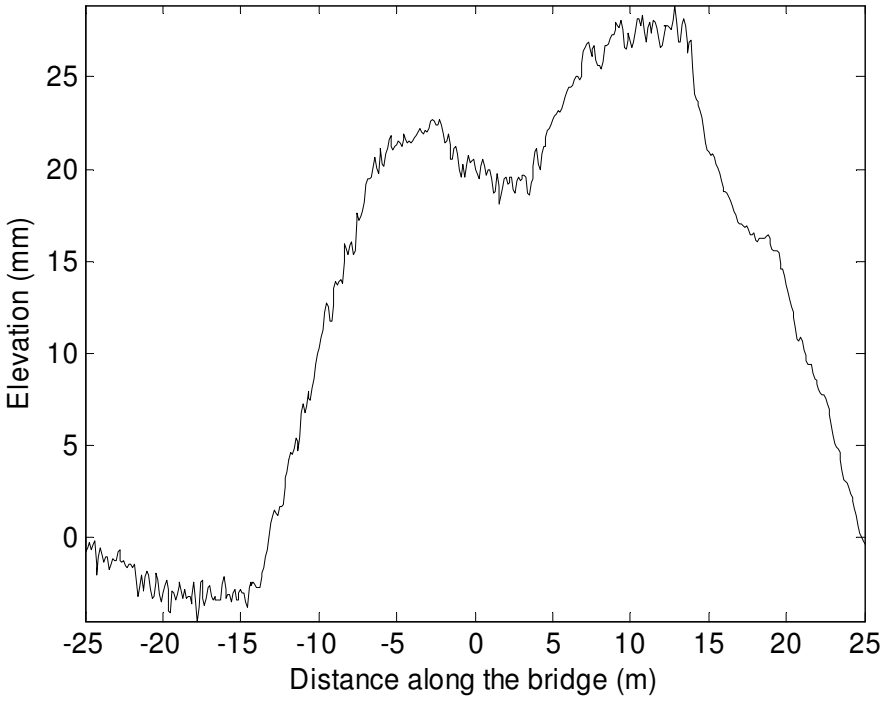
Elevation (mm)
25
20
15
10
5
0
-25
-20
-15
-10
-5
0
5
10
15
20
25
Distance along the bridge (m)

Fig. 3

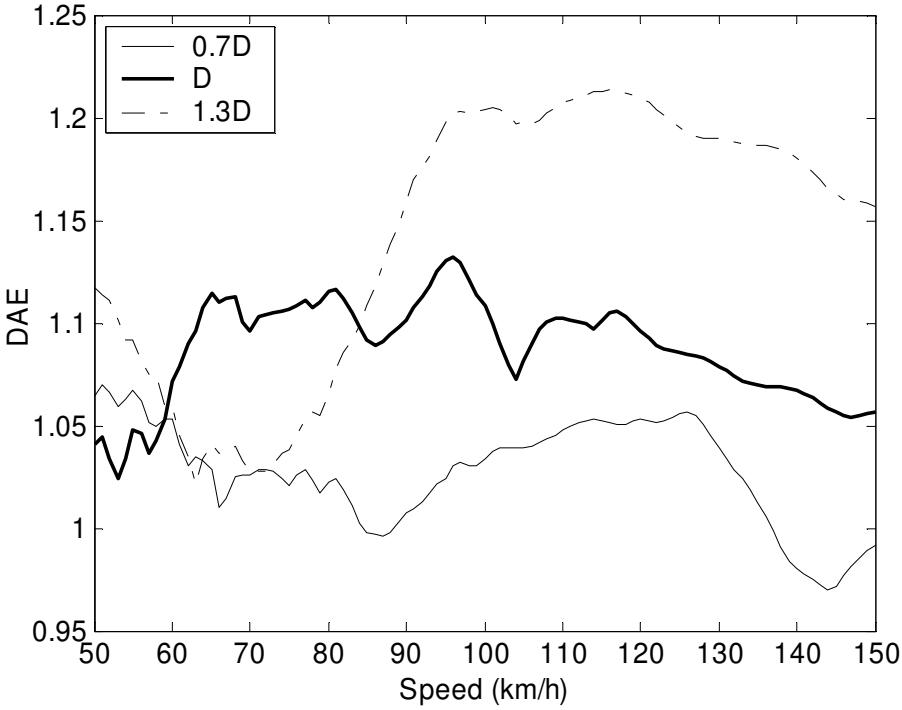
0.7D
D
1.3D
DAE
Speed (km/h)
1.25
1.2
1.15
1.1
1.05
1
0.95
50
60
70
80
90
100
110
120
130
140
150

Fig. 4

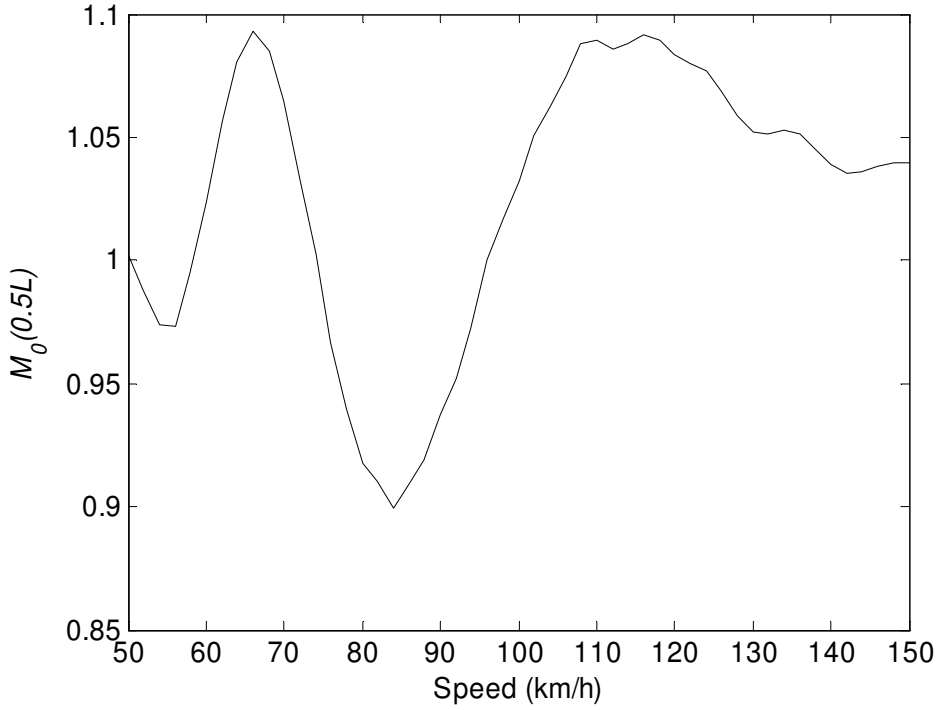
1.1
1.05
1
0.95
0.9
0.85
$M_0(0.5L)$
50
60
70
80
90
100
110
120
130
140
150
Speed (km/h)

(a)

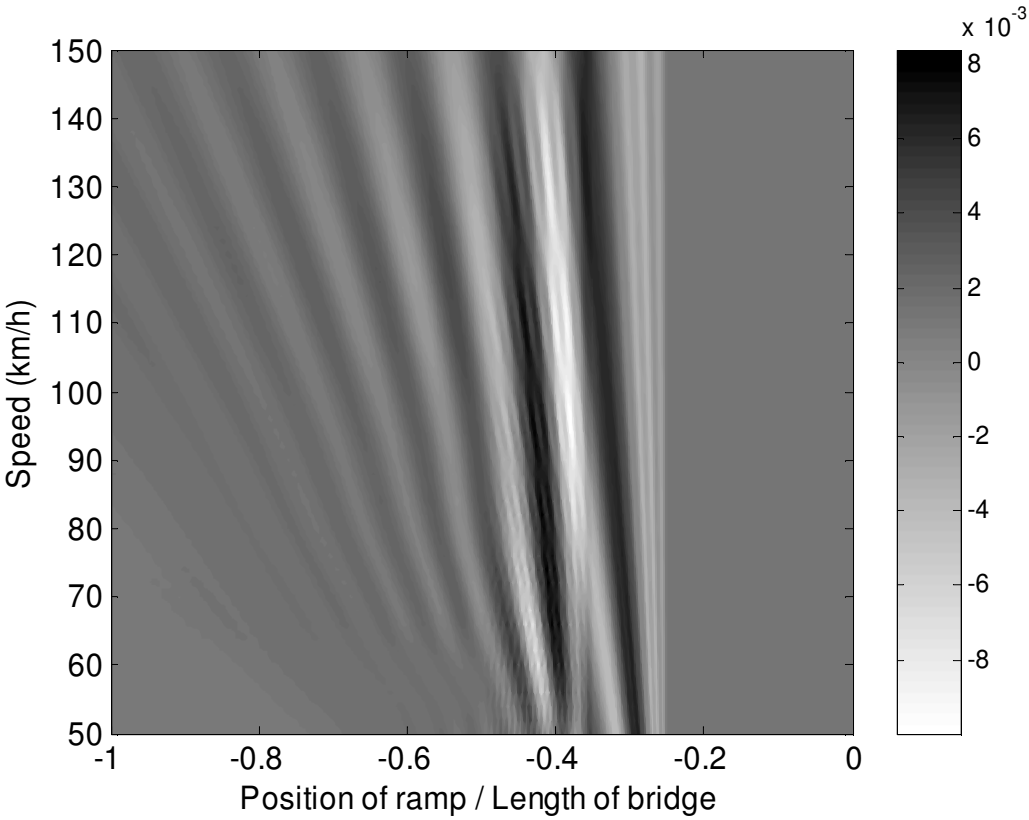
x 10^{-3}
8
6
4
2
0
-2
-4
-6
-8
150
140
130
120
110
100
90
80
70
60
50
Speed (km/h)
-1
-0.8
-0.6
-0.4
-0.2
0
Position of ramp / Length of bridge

(b)

Fig. 5

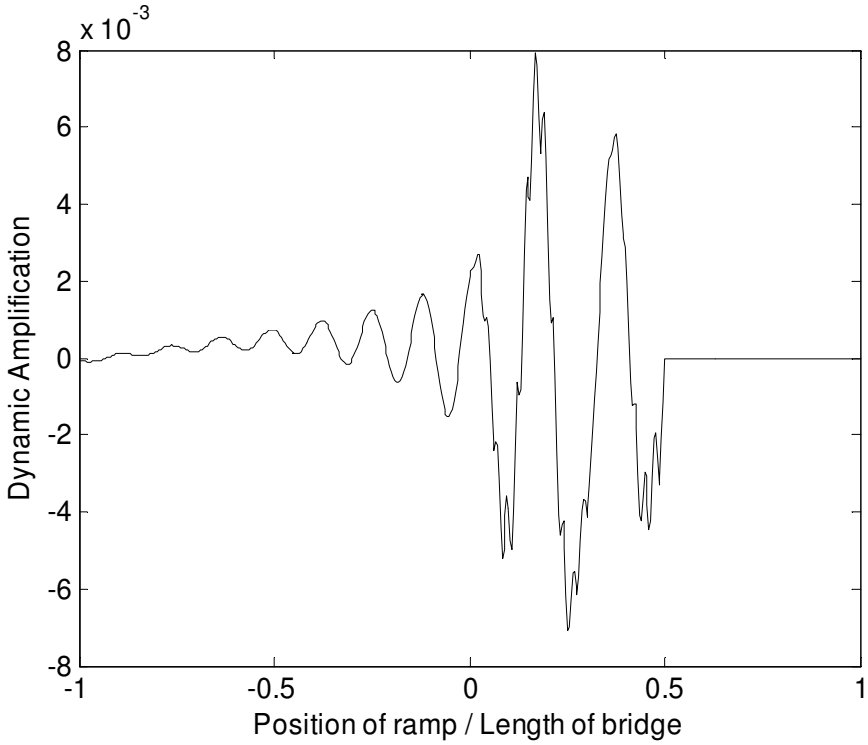
x 10^-3
8
6
4
2
0
-2
-4
-6
-8
Dynamic Amplification
-1
-0.5
0
0.5
1
Position of ramp / Length of bridge

(a)

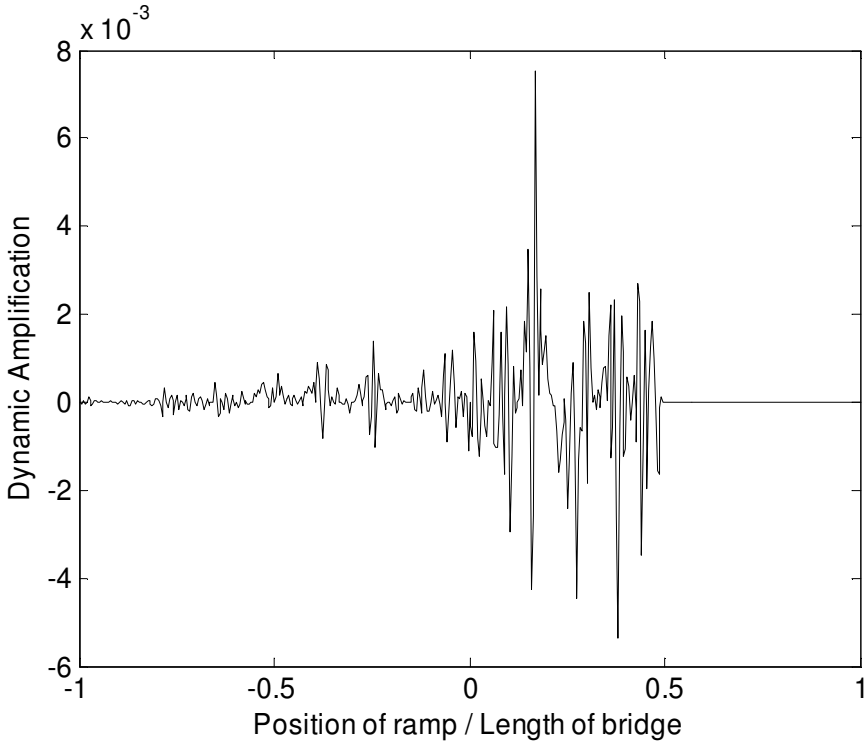
x 10^-3
8
6
4
2
0
-2
-4
-6
Dynamic Amplification
-1
-0.5
0
0.5
1
Position of ramp / Length of bridge

(b)

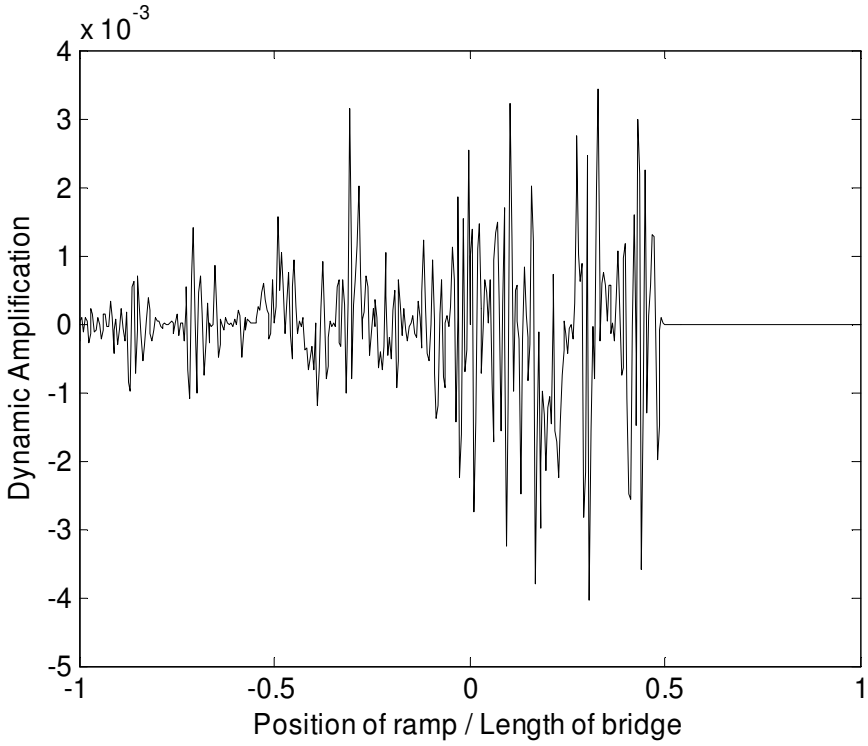
x 10^-3
4
3
2
1
0
-1
-2
-3
-4
-5
Dynamic Amplification
-1
-0.5
0
0.5
1
Position of ramp / Length of bridge

(c)

Fig. 6

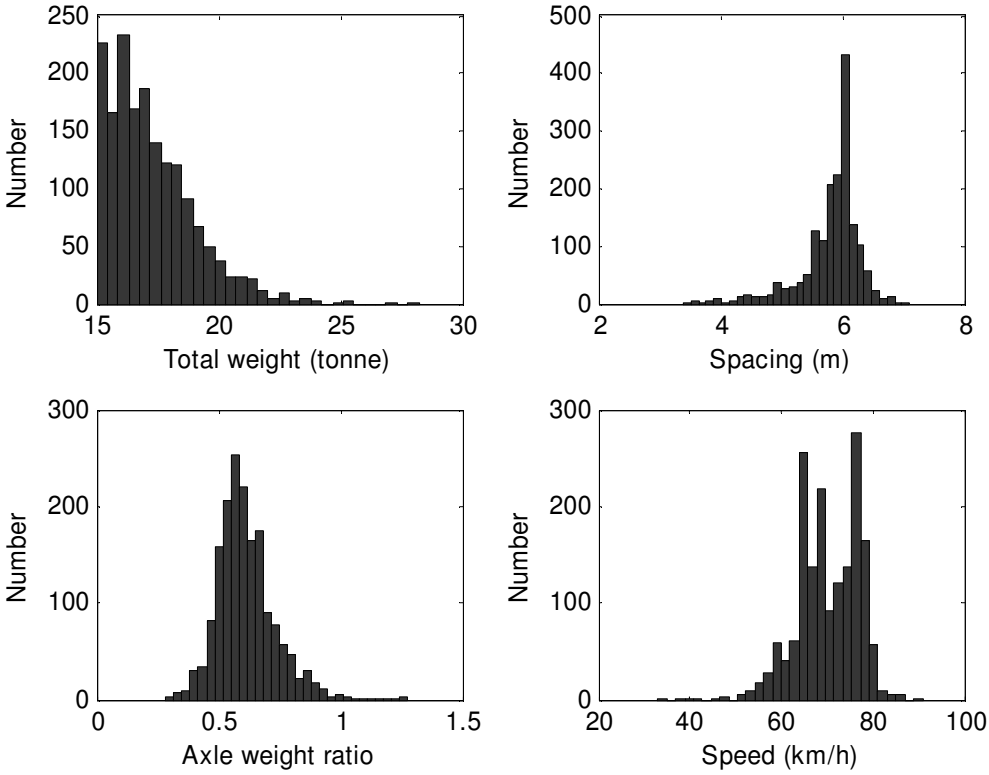
Number
Total weight (tonne)
Spacing (m)
Axle weight ratio
Speed (km/h)

Fig. 7

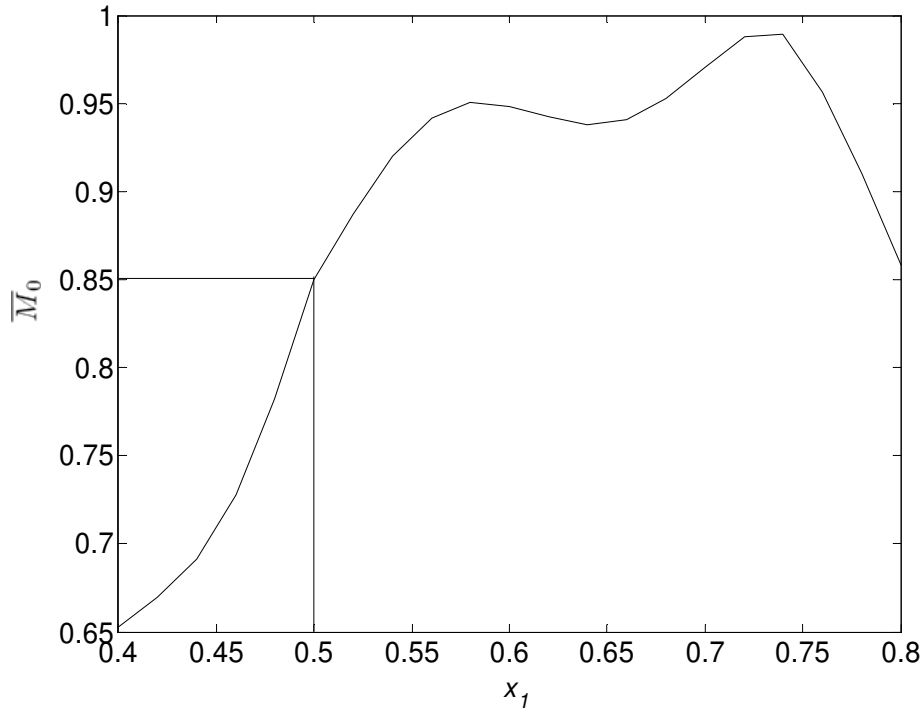
1
0.95
0.9
0.85
0.8
0.75
0.7
0.65
$\overline{M}_0$
0.4
0.45
0.5
0.55
0.6
0.65
0.7
0.75
0.8
x_1

(a)

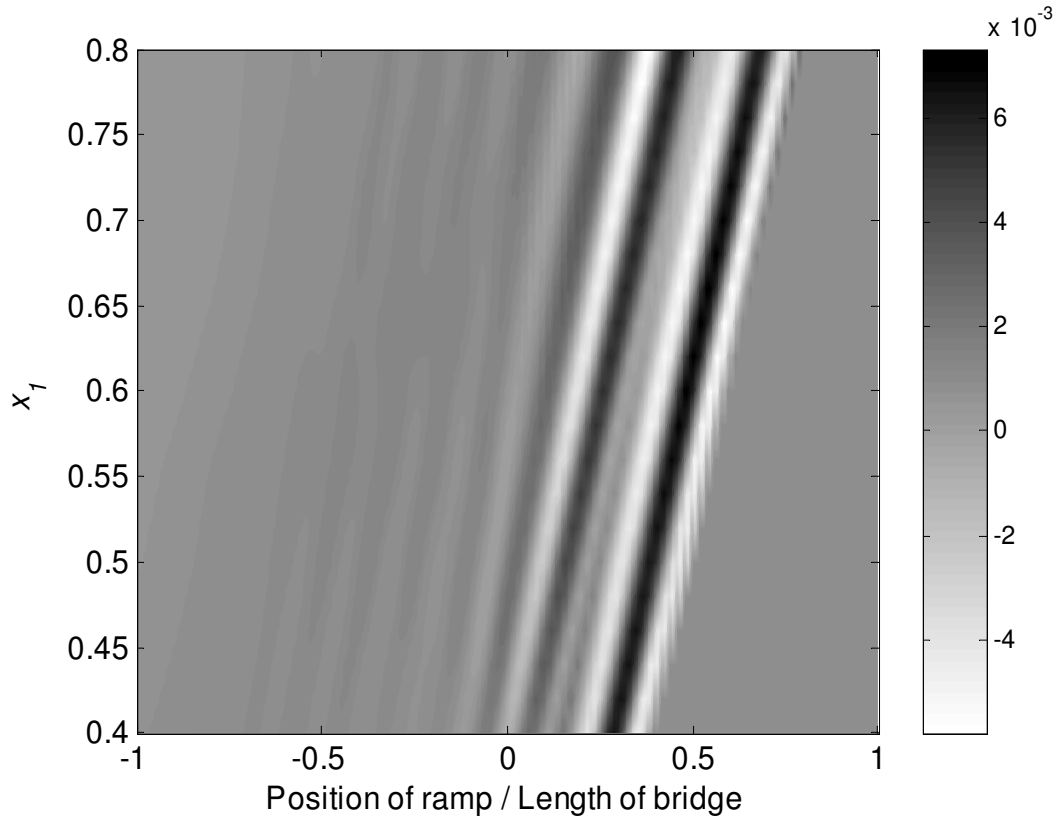
x 10^-3
6
4
2
0
-2
-4
0.8
0.75
0.7
0.65
0.6
0.55
0.5
0.45
0.4
x_1
-1
-0.5
0
0.5
1
Position of ramp / Length of bridge

(b)

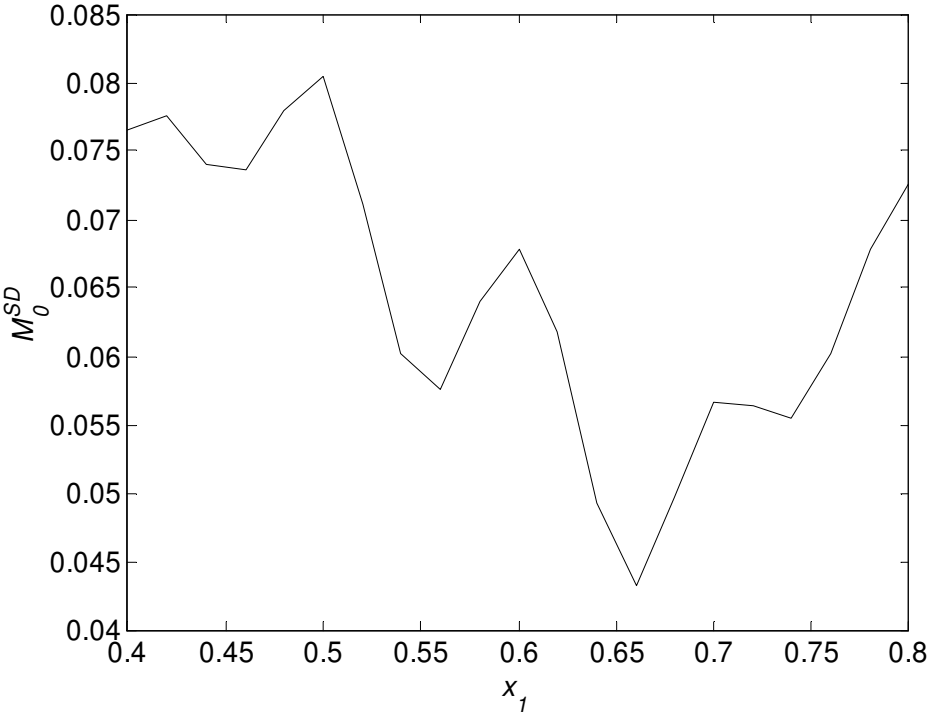
0.085
0.08
0.075
0.07
0.065
0.06
0.055
0.05
0.045
0.04
M_0^{SD}
0.4
0.45
0.5
0.55
0.6
0.65
0.7
0.75
0.8
x_1

(c)

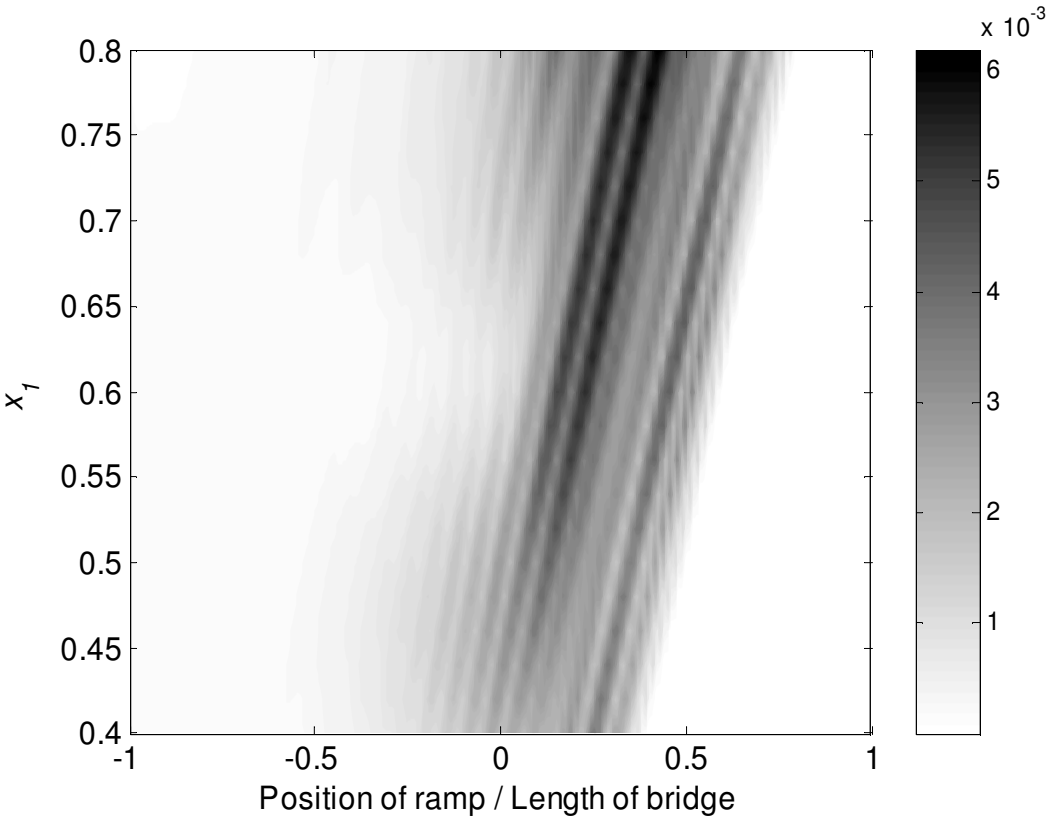
x 10^-3
6
5
4
3
2
1
0.8
0.75
0.7
0.65
0.6
0.55
0.5
0.45
0.4
x_1
-1
-0.5
0
0.5
1
Position of ramp / Length of bridge

(d)

Fig. 8

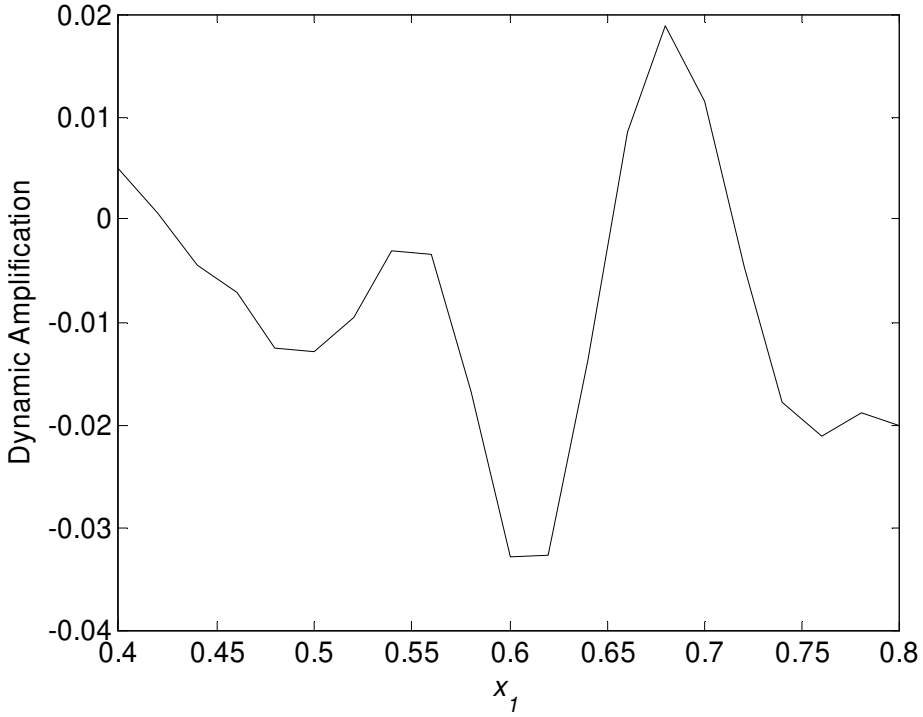
0.02
0.01
0
-0.01
-0.02
-0.03
-0.04
Dynamic Amplification
0.4
0.45
0.5
0.55
0.6
0.65
0.7
0.75
0.8
x_1

(a)

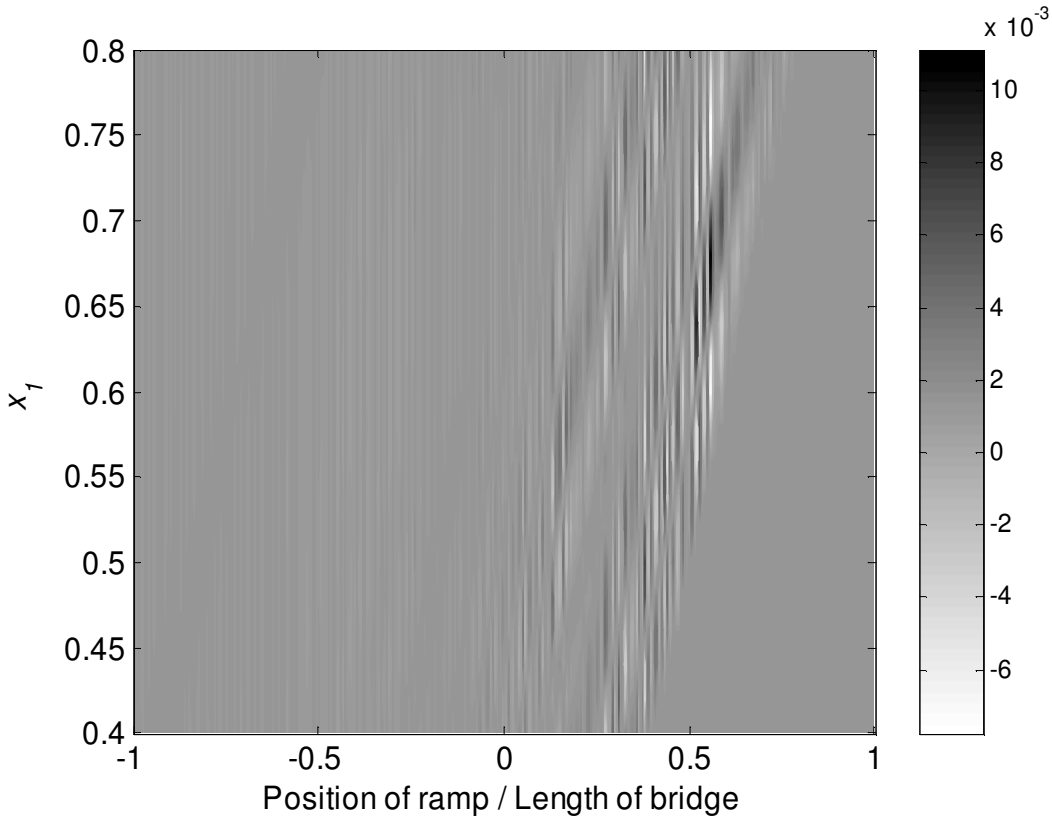
x 10^-3
10
8
6
4
2
0
-2
-4
-6
0.8
0.75
0.7
0.65
0.6
0.55
0.5
0.45
0.4
x_1
-1
-0.5
0
0.5
1
Position of ramp / Length of bridge

(b)

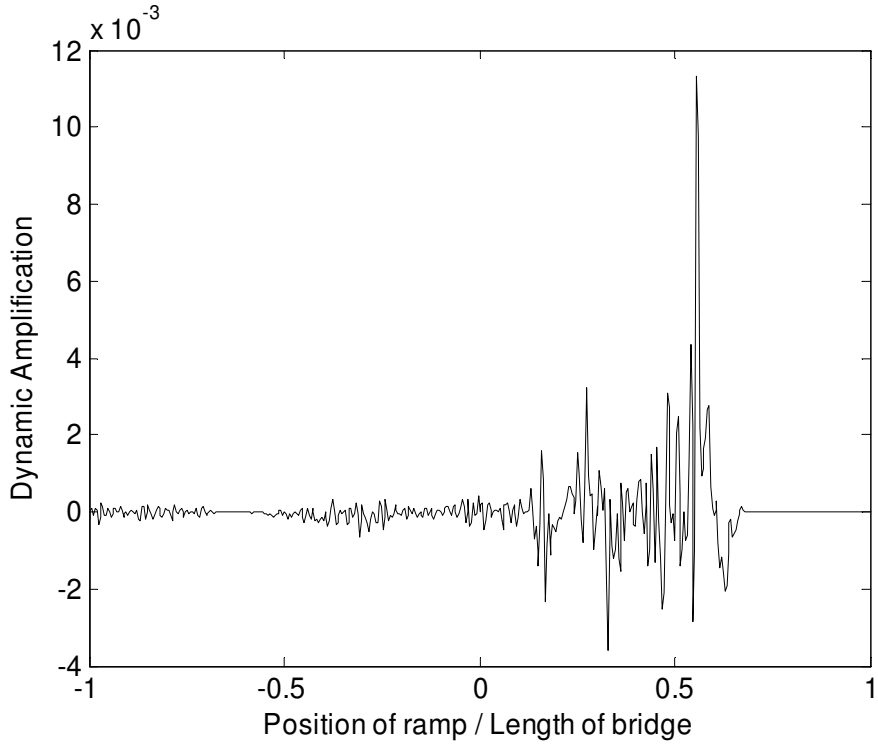
x 10^-3
12
10
8
6
4
2
0
-2
-4
Dynamic Amplification
-1
-0.5
0
0.5
1
Position of ramp / Length of bridge

(c)

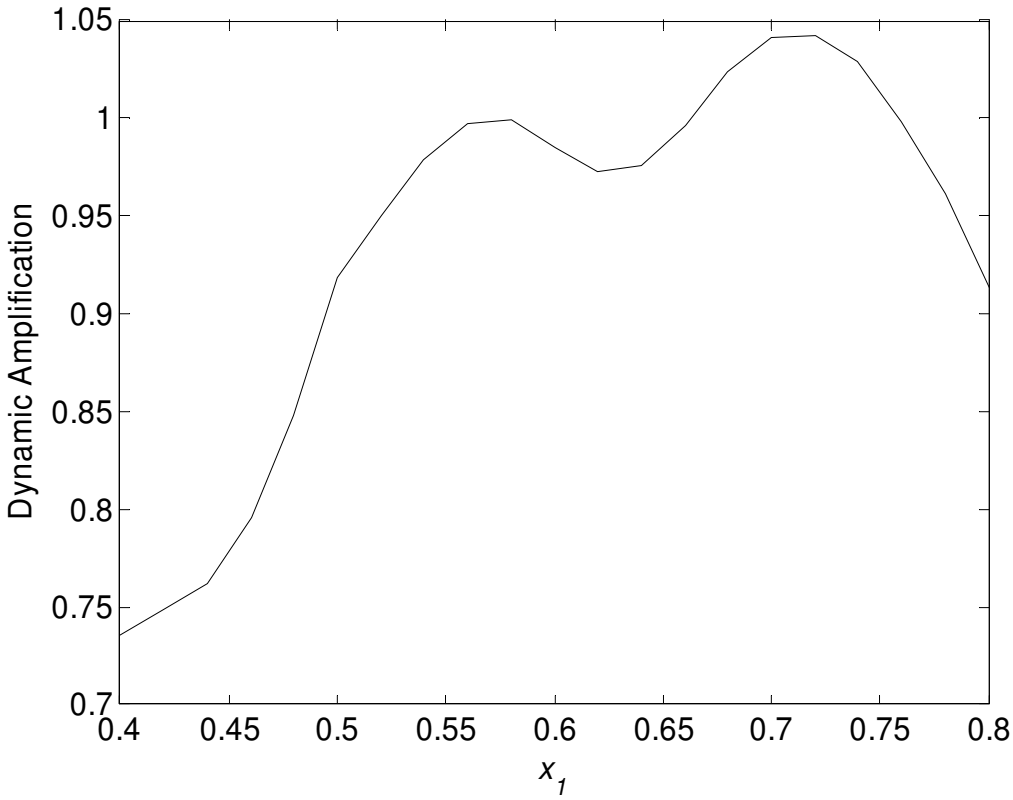
1.05
1
0.95
0.9
0.85
0.8
0.75
0.7
Dynamic Amplification
0.4
0.45
0.5
0.55
0.6
0.65
0.7
0.75
0.8
x1

(d)

Fig. 9

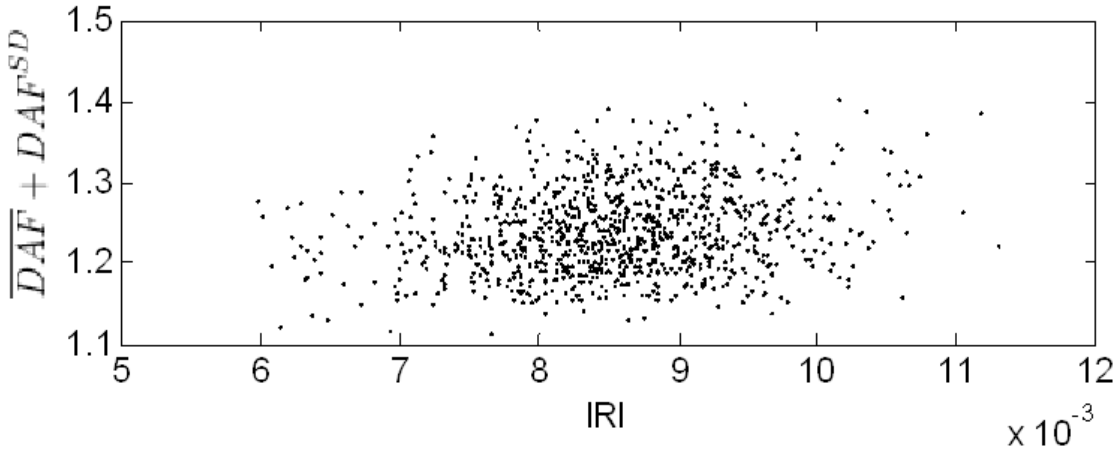
1.5
1.4
1.3
1.2
1.1
5
6
7
8
9
10
11
12
IRI
x 10^-3
$\overline{DAF} + DAF^{SD}$

(a)

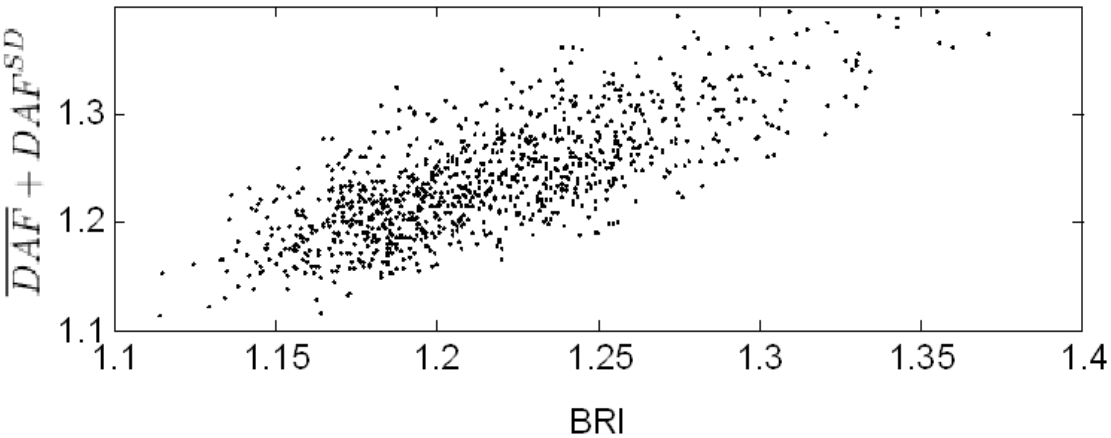
1.3
1.2
1.1
1.1
1.15
1.2
1.25
1.3
1.35
1.4
BRI
$\overline{DAF} + DAF^{SD}$

(b)

Fig. 10

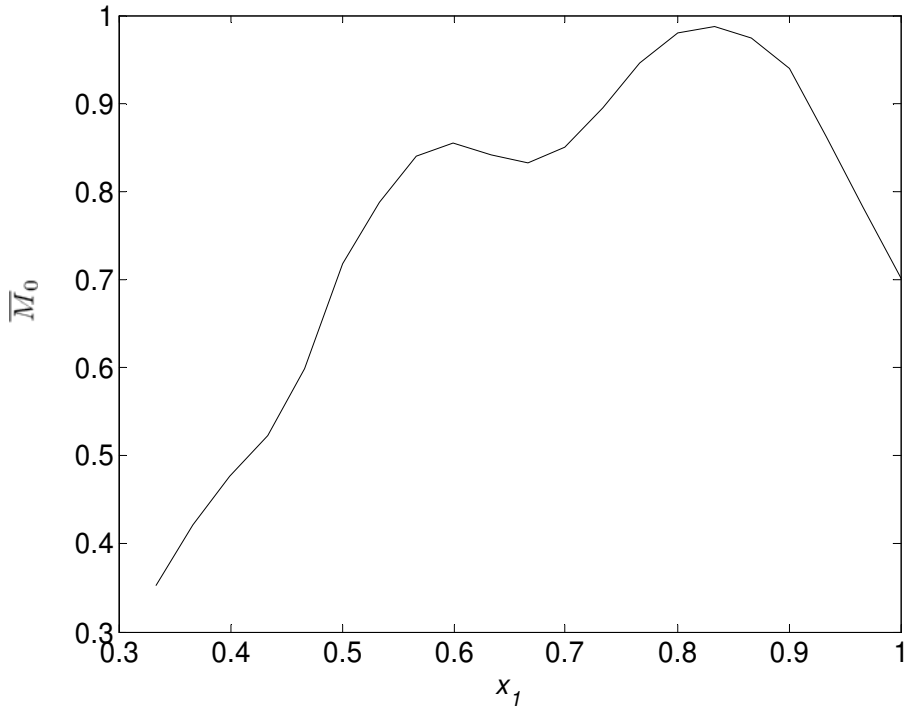
1
0.9
0.8
0.7
0.6
0.5
0.4
0.3
$\overline{M}_0$
0.3
0.4
0.5
0.6
0.7
0.8
0.9
1
x_1

(a)

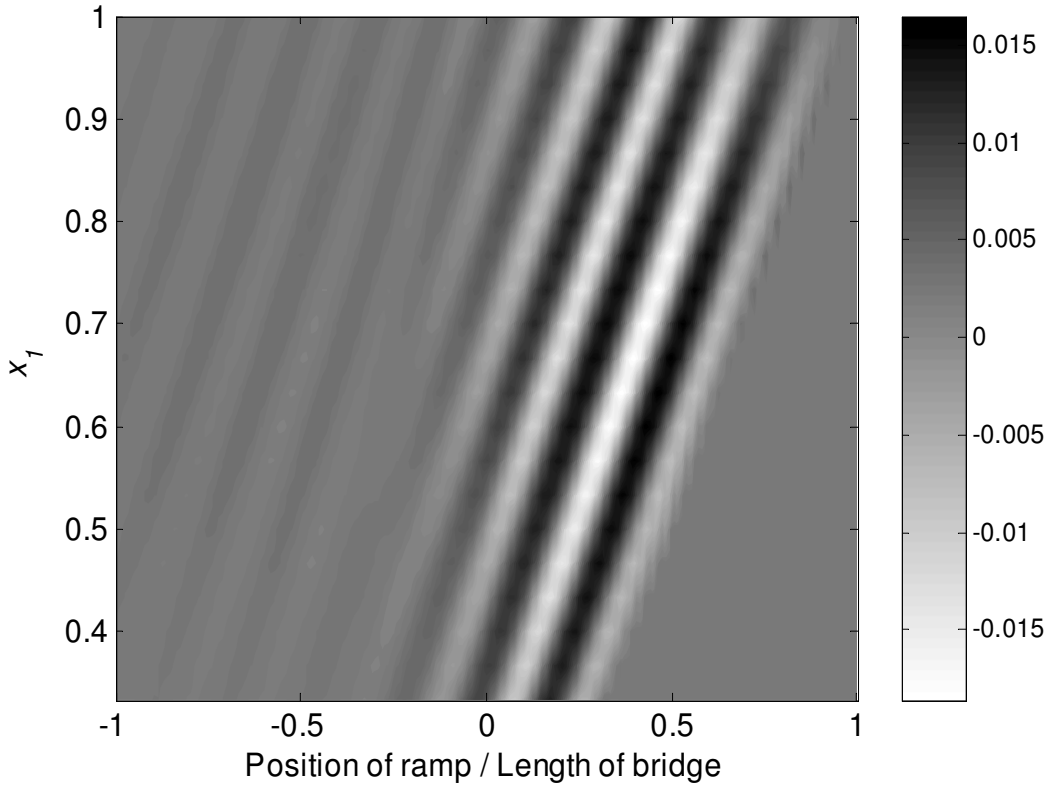
1
0.9
0.8
0.7
0.6
0.5
0.4
x_1
-1
-0.5
0
0.5
1
Position of ramp / Length of bridge
0.015
0.01
0.005
0
-0.005
-0.01
-0.015

(b)

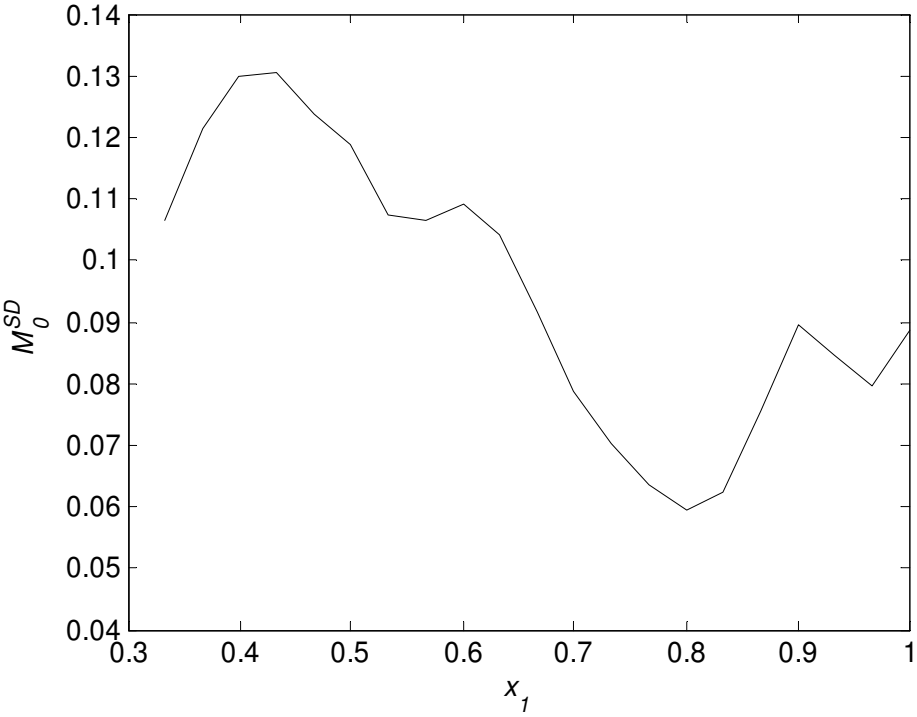
0.14
0.13
0.12
0.11
0.1
0.09
0.08
0.07
0.06
0.05
0.04
M_0^{SD}
0.3
0.4
0.5
0.6
0.7
0.8
0.9
1
x_1

(c)

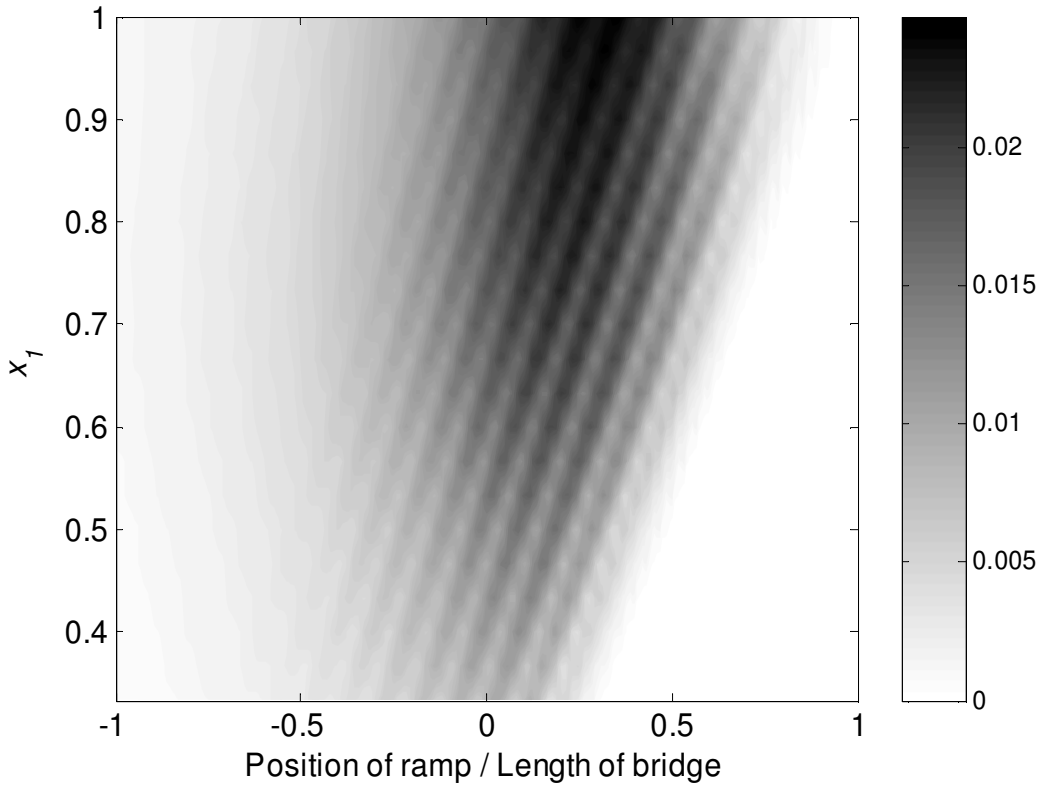
1
0.9
0.8
0.7
0.6
0.5
0.4
x_1
-1
-0.5
0
0.5
1
Position of ramp / Length of bridge
0.02
0.015
0.01
0.005
0

(d)

Fig. 11

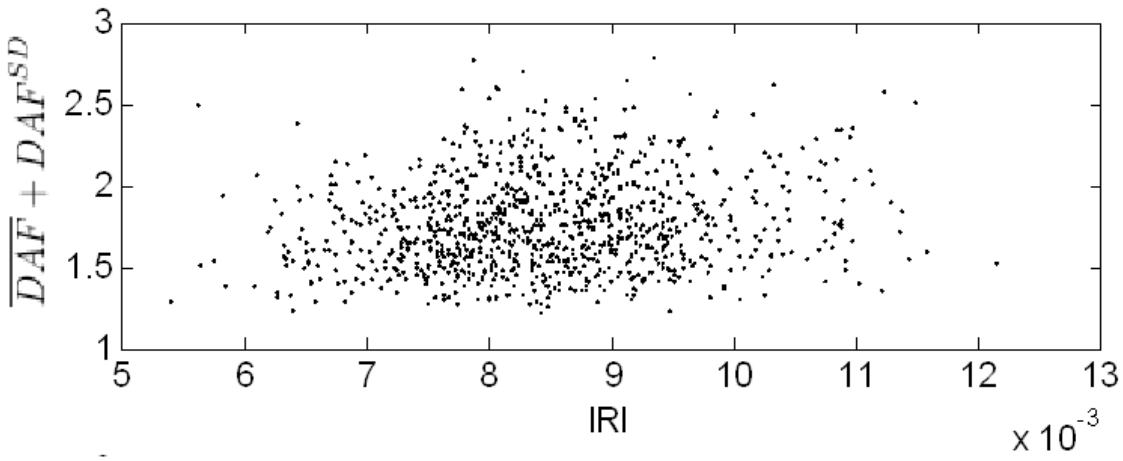

(a)

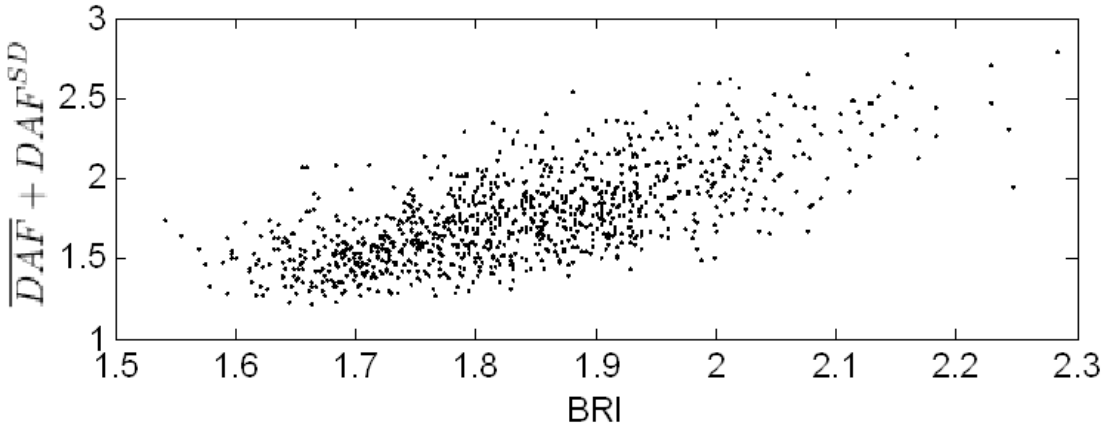

(b)

Fig. 12

Vehicle Properties		
Physical description	symbol	Value
Sprung mass	m_3	18000 kg

Beam Properties		
Physical description	symbol	Value
Mass per unit length	μ	18358 kg/m

Unsprung mass	m_1, m_2	1000 kg
Suspension stiffness	K_s	80 kN/m
Tire vertical stiffness	K_t	1800 kN/m
Passive damping coefficient	C	7 kNs/m
Distance between the axles to center of gravity	D_i	2.5 m

Moment of inertia of beam cross-section	J	1.3901 m^4
Bridge Length	l	25 m
Young's modulus of beam	E	3.5×10^{10} N/m^2

Table 1. Vehicle and Beam Properties.